Available online at www.sciencedirect.com
ScienceDirect
Journal of Nuclear Materials 367–370 (2007) 60–67
journal of nuclear materials
www.elsevier.com/locate/jnucmat

Recent progress in US–Japan collaborative research on ferritic steels R&D

Akihiko Kimura [a,*], Ryuta Kasada [a], Akira Kohyama [a], Hiroyasu Tanigawa [b], Takanori Hirose [b], Kiyoyuki Shiba [b], Shiro Jitsukawa [b], Satoshi Ohtsuka [c], Shigeharu Ukai [c], M.A. Sokolov [d], R.L. Klueh [d], Takuya Yamamoto [e], G.R. Odette [e]

[a] *Institute of Advanced Energy, Kyoto University, Gokasho, Uji, Kyoto 611-0011, Japan*
[b] *Japan Atomic Energy Research Institute, Tokai, Naka-gun, Ibaraki, Japan*
[c] *Japan Nuclear Cycle Development Institute, Oarai, Higashiibaraki-gun, Ibaraki, Japan*
[d] *Oak Ridge National Laboratory, Oak Ridge, TN, USA*
[e] *University of California at Santa Barbara, Santa Barbara, CA, USA*

Abstract

The mechanisms of irradiation embrittlement of two Japanese RAFSs were different from each other. The larger DBTT shift observed in F82H is interpreted by means of both hardening effects and a reduction of cleavage fracture stress by $M_{23}C_6$ carbides precipitation along lath block and packet boundaries, while that of JLF-1 is due to only the hardening effect. Dimensional change measurement during in-pile creep tests revealed the creep strain of F82H was limited at 300 °C. Performance of the weld bond under neutron irradiation will be critical to determine the life time of blanket structural components. Application of the ODS steels, which are resistant to corrosion in supercritical pressurized water, to the water-cooled blanket is essential to increase thermal efficiency of the blanket systems beyond DEMO. The coupling of RAFS and ODS steel could be effective to realize a highly efficient fusion blanket.

1. Introduction

Despite of the variety of proposed systems for the International Thermonuclear Experimental Reactor (ITER) Test Blanket Modules (TBM), reduced activation ferritic steel (RAFS) was selected as the only candidate for the structural material [1]. This clearly indicates the higher priority of RAFS over the other materials candidates as a fusion blanket structural material. The US proposed systems that utilize lead–lithium as a breeder and/or coolant [2,3]. Japan proposed a variety of systems cooled by water [4], helium gas [5], lead–lithium [6], lithium [7] or molten salt [8]. Each party, however, selected RAFS as the structural material of the TBMs.

Two US–Japan collaborative research programs on RAFS have been carried out in parallel for several years. One is the so-called 'Phase IV' program of the

* Corresponding author. Tel.: +81 774 38 3476; fax: +81 774 38 3479.
E-mail address: Kimura@iae.kyoto-u.ac.jp (A. Kimura).

0022-3115/$ - see front matter © 2007 Elsevier B.V. All rights reserved.
doi:10.1016/j.jnucmat.2007.03.013

US-DOE (Department of Energy)/JAEA (Japan Atomic Energy Agency) collaborative research on reduced activation ferritic steels, which is characterized by irradiation experiments to provide the basic irradiation database required for fusion blanket design, including the effects of neutron irradiation on the mechanical properties, dimensional stabilities, microstructures and so on. The other is the 'JUPITER-II' program of US-DOE/MEXT (Ministry of Education, Culture, Sports, Science and Technology) collaborative research on fusion blanket technology led by Japanese universities and is focused on the liquid breeder blanket system–material integration studies on the synergistic effects of corrosion, helium and neutron irradiation in fusion relevant environment.

The IEA-heat of F82H is the first candidate Japanese RAFS, and the database has been compiled under the US/Japan collaborative efforts. In this paper, recent progress in US–Japan collaborative research on ferritic steels R&D is reviewed with a focus on ITER–TBM fabrication and DEMO blanket design.

2. Irradiation embrittlement mechanisms

2.1. Difference in $\Delta DBTT$ and $\Delta\sigma_y$ between F82H and JLF-1

The fracture toughness measurement after HFIR irradiation at 300 °C to 5 dpa revealed that a much larger ductile brittle transition temperature (DBTT) shift was observed for F82H than for JLF-1 [9]. The main differences between these steels is the Cr, Ta and N concentrations and heat treatment conditions as shown in Table 1 in which the compositions of the Mod. JLF-1 are also shown. The DBTT before irradiation is 190 K and 215 K for JLF-1 and F82H, respectively. The dependence of ΔDBTT and $\Delta\sigma_y$ on the irradiation temperature for F82H and JLF-1 is shown in Fig. 1. In both steels, the DBTT shift decreases with increasing irradiation temperature,

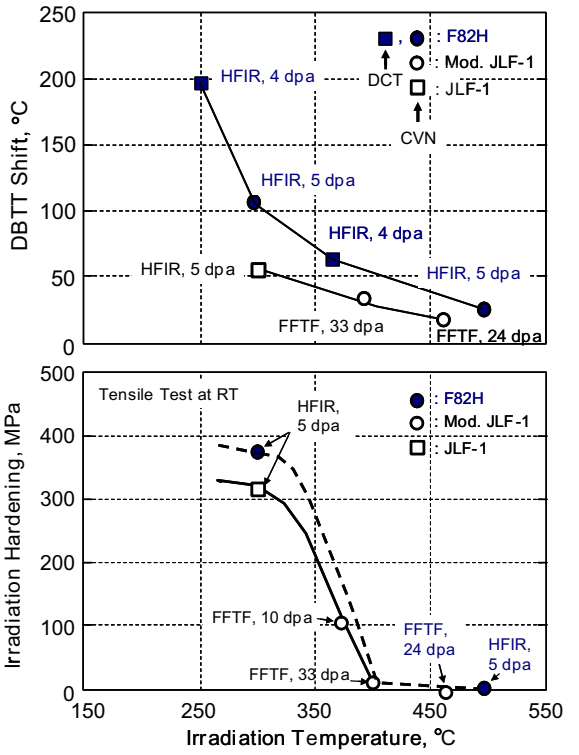

Fig. 1. The dependence of ΔDBTT and $\Delta\sigma_y$ on the irradiation temperature in F82H and JLF-1.

and the irradiation hardening appears to decrease with increasing irradiation temperature up to around 400 °C, and then it disappears. The DBTT shift of F82H is twice that of JLF-1 at all the tested irradiation temperatures, while the irradiation hardening of the steels is not significantly different, although the hardening of JLF-1 appears to be a little bit smaller than that of F82H. It has been considered that the DBTT shift of RAFS is generally interpreted in terms of a 'hardening mechanism' when they break in a cleavage fracture mode, and there is a linear relationship between ΔDBTT and $\Delta\sigma_y$. The data obtained after irradiation at 300 °C indicates that F82H exhibits a higher potential for embrittlement than JLF-1 at the same hardening.

Table 1
Chemical compositions and heat treatment conditions of F82H and JLF-1

	C	Si	Mn	P	S	Cr	W	V	Ta	Ti	B	N
F82H	0.093	0.09	0.21	0.004	0.0014	7.46	1.96	0.15	0.023	–	–	0.006
JLF-1	0.097	0.05	0.46	0.002	0.0020	9.04	1.97	0.19	0.073	0.001	–	0.05
Mod.JLF-1	0.10	0.042	0.53	0.002	0.0014	9.03	2.06	0.26	0.051	0.021	0.0032	0.10

F82H: normalized at 1040 °C for 30 min and then tempered at 750 °C for 1 h, AC; JLF-1: normalized at 1050 °C for 30 min and then tempered at 775 °C for 1 h, AC; Mod. JLF-1: normalized at 1050 °C for 30 min and then tempered at 760 °C for 1 h, AC.

2.2. Irradiation hardening mechanisms

It has been reported that the factors controlling irradiation hardening of RAFS are irradiation-induced dislocation loops, precipitates and microvoids [10–19]. The contribution of each factor on the hardening depends on material. It was shown that the irradiation hardening of mod. JLF-1 is mainly due to dislocation loops [16,20]. Fig. 2 shows dislocation structures and precipitates observed in the steel after neutron irradiation at 370 °C up to 10 dpa, indicating that $\boldsymbol{b} = \boldsymbol{a}\langle 1\,0\,0\rangle$ type dislocation loops and very fine precipitates were observed after the irradiation ($M_{23}C_6$ and possibly MX). Since both structures were considered to be a cause of the hardening, the following measurements were carried out to evaluate each contribution to the hardening. Fig. 3 shows the comparison of the irradiation hardening measured in tensile tests and values estimated from the microstructure calculated using the dispersed barrier model, where the barrier strength was assumed to be 0.23 and 0.30 for dislocation loops and precipitates, respectively. The tensile tests and microstructural observations were performed in the as-irradiated condition and after the post-irradiation annealing at 400, 500 and 600 °C for 1 h. The contribution of each structure to the irradiation hardening was expressed by the following equation:

$$\Delta\sigma^2_{\mathrm{Total}} = \Delta\sigma^2_{\mathrm{Loop}} + \Delta\sigma^2_{\mathrm{Prec}}. \quad (1)$$

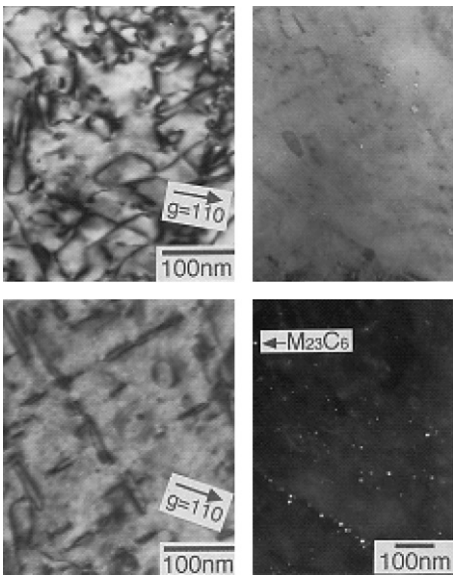

Fig. 2. The dislocation structures and precipitates observed in Mod. JLF-1 after neutron irradiation at 370 °C up to 10 dpa.

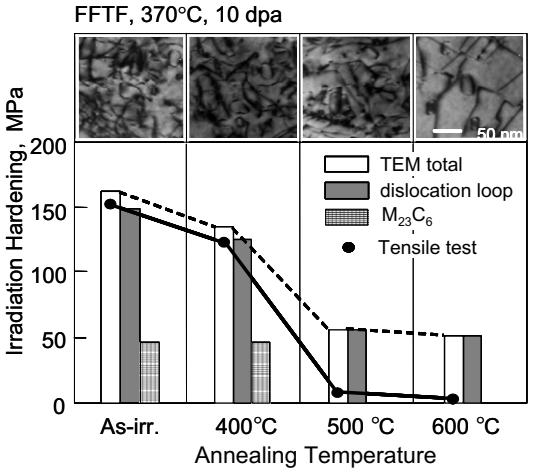

Fig. 3. Comparison of the irradiation hardening from tensile test results and estimated values from the microstructure using the dispersed barrier model.

The irradiation hardening was decreased by annealing which caused recovery of the dislocation loops as shown in the micrographs in the top of Fig. 3. Small black dots, which are considered to be small loops or precipitates, also disappeared during the annealing. The contribution of dislocation loops to the hardening was dominant, and the hardening was almost accounted for by a dislocation loop hardening mechanism. As for the role of microvoids on the hardening, our previous work [21] clearly indicated that it was small and less than 10% of the contribution from dislocation loops.

2.3. Irradiation embrittlement mechanisms

Although the irradiation hardening of F82H and JLF-1 is similar, F82H shows a larger ΔDBTT. This can be interpreted in terms of reduction of fracture stress in F82H. It is expected that the irradiation-induced changes in the precipitation morphology results in the reduction of cleavage fracture stress and consequently increases the ΔDBTT. Although the grain size is different between the steels, the previous research showed the ΔDBTTs of fine and coarse grained F82H steels were almost the same [22].

Since carbides may be the nucleation sites for brittle cleavage fracture that determines DBTT, the difference in their irradiation-induced precipitation behavior was investigated for F82H, JLF-1 and ORNL-9Cr steels to understand the difference in the DBTT shift among the steels [23]. The structures and chemical compositions of the extracted

Table 2
Summary of the results obtained for F82H and JLF-1

HFIR irradiation, 300 °C, 5 dpa	F82H	JLF-1
Irradiation hardening (RT)	370 MPa	314 MPa
DBTT before irradiation	215 K	190 K
Shift in DBTT	110 K	40 K
Loop density	6.64E + 23/m^3	5.91E + 23/m^3
Loop size (average)	3.5 nm	3.6 nm
Estimated from dispersed barrier model	310 MPa	300 MPa
Precipitates (extrusion residue) a measure of large precipitates	Total amount increased	Total amount decreased
Precipitates (TEM), a measure of precipitation location	Fraction of prec. Increased at block and PAG boundaries	Small $M_{23}C_6$, small MX in matrix
Main factor controlling hardening	Loops	Loops
Main factor controlling DBTT shift	Hardness and carbides	Hardness

precipitate residues from the steels were investigated. The main results obtained suggested that in JLF-1 and ORNL steels, large MX (TaC) carbides disappeared during irradiation, while they were observed in F82H [23]. A TEM observation revealed that the volume fraction of the $M_{23}C_6$ that precipitated along lath block and packet boundaries to the total volume of the $M_{23}C_6$ was twice as large for F82H than JLF-1. It is expected that the fracture stress along lath block and packet boundaries is reduced by the precipitation of $M_{23}C_6$ carbides. The experimental results are summarized in Table 2 along with the mechanisms of irradiation hardening and embrittlement.

The effects of tempering heat treatment condition on the irradiation hardening were investigated for F82H. The materials were tempered at different conditions and irradiated in JMTR at 300 °C to 2 dpa. The DBTT shift was considerably influenced by the tempering temperature [24].

3. Dimensional stability

3.1. In-pile creep

Creep tube specimens were fabricated from F82H and JLF-1 series steels and irradiated in HFIR at 300 °C up to 5 dpa (for 526 days). In-pile creep strain was determined by measuring the diameters of the tubes pressurized to each hoop stress level after irradiation, and is shown in Fig. 4. Below the hoop stress of 350 MPa, no significant difference in the creep strain was observed among the steels tested. The in-pile creep strain at 300 °C of the steels was 0.12% at a hoop stress of 320 MPa. At high hoop stresses, over 375 MPa, a significant large creep strain was observed for JLF-1which is considered to be due to the applied stress exceeding the yield stress.

3.2. Swelling by dual beam ion irradiation

The effects of helium on swelling in JLF-1 has been investigated by means of dual beam irradiation where iron ions and helium ions were simultaneously introduced at 470 °C up to 80 dpa. Fig. 5 shows the dependence of the void swelling of JLF-1 irradiated with dual ion beams [25,26] as well as

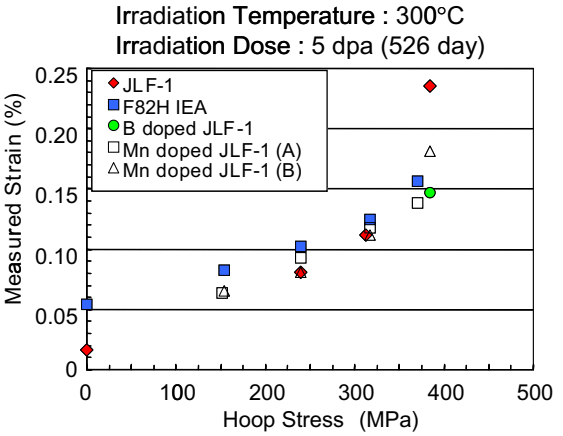

Fig. 4. The dependence of in-pile creep strain on hoop stress of the steels irradiated at 300 °C.

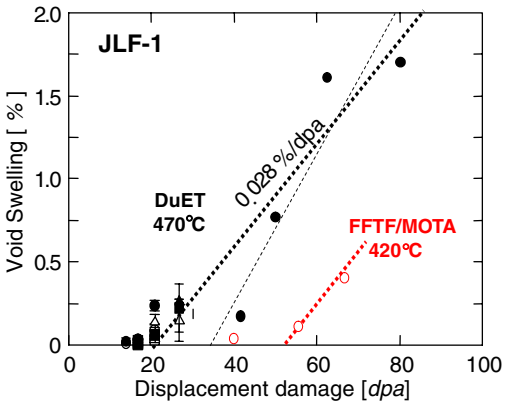

Fig. 5. The dependence of the void swelling of JLF-1 irradiated with dual ion beam [20,21] as well as the results obtained for the steel irradiated with neutrons at 420 °C [22].

the results obtained for the steel irradiated with neutrons at 420 °C [27]. The swelling peak temperature of the steel depends upon the type of irradiation. In case of the ion irradiation, the swelling peak temperature was measured to be around 470 °C, while it was around 420 °C for the case of neutron irradiation in fast reactors, which is due to the difference in the damage rate. There are two characteristic features in the dose dependence: (1) an incubation dose, and (2) on almost linear dependence with a slope of 0.028%/dpa above it. The incubation dose was 20 dpa and 50 dpa for ions and neutrons irradiation, respectively. A higher damage rate could enhance the occurrence of swelling.

4. Joining/welding techniques

A blanket structure is generally complex. Even a simple structure demands rather high performance of joints and welds. The mechanical properties of TIG and EB welds were investigated for F82H. Fig. 6 (TIG weld) and Fig. 7 (EB weld) show metallographic photos of the welds of F82H-IEA heat and their mechanical properties. Tensile specimens were fabricated from the TIG weld bond. The specimens obtained from the weld metal showed a higher yield stress than base metal at all the test temperatures. The specimens denoted as TIG/WJ were fabricated so that the heat affected zone (HAZ) area was located in the gage section of the tensile specimens. It is clear that there is a soft area in the HAZ of the TIG weld where the yield stress is

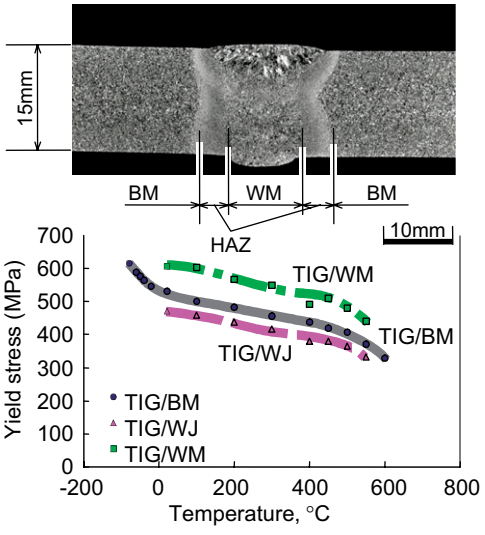

Fig. 6. Metallographic photo of the TIG weld of F82H-IEA heat and its mechanical properties.

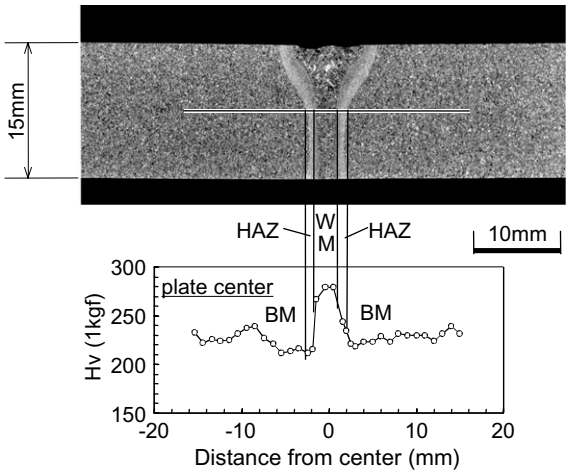

Fig. 7. Metallographic photo of the EB weld of F82H-IEA heat and its mechanical properties.

about 50 MPa lower than the base metal. This behavior is similar to a reactor pressure vessel steel, A533B steel [28,29], which showed that there is a soft area in the HAZ of an A533B sub-merged arc weld. It is of note that the soft area is not ductile but it shows the highest DBTT despite the lowest yield stress. The width of EB weld bond is much narrower than that of TIG weld, and also the weld metal is harder than base metal.

The surveillance tests on the effects of irradiation on the hardness and DBTT of welds is essential for the design and practical fabrication of the blanket. Again, the studies on A533B [28,29] revealed that the weld metal and soft area of HAZ suffered the largest DBTT shift by neutron irradiation. Consequently, the DBTT of the A533B steel weld is determined by the DBTT of the weld metal that showed highest DBTT.

ITER operation condition indicates the importance of fatigue database because of the pulse mode operation and occurrence of severe plasma disruptions. Fatigue properties of the weld that has a soft area could be one of the critical issues for blanket structure, because the fatigue life of an irradiated weld is to be determined by the weakest soft area.

5. Compatibility to super-critical pressurized water

5.1. Resistance to stress corrosion cracking

High temperature SCPW (super critical pressurized water) is an attractive option from the viewpoint of higher thermal efficiency. F82H has been

tested to investigate the susceptibility to stress corrosion cracking (SCC) by means of slow strain rate tests (SSRT) at a strain rate of 3×10^{-7} s^{-1} in a flowing (flow rate: 6×10^{-7} m^3 s^{-1}) SCPW environment, at a pressure of 23.5 MPa at temperatures between 280 and 550 °C in a solution with a dissolved oxygen of 0.2–0.3 wt ppm [30]. For comparison, the deformation behavior at a strain rate of 5×10^{-5} s^{-1} was also investigated, and both are shown in Fig. 8. Tensile properties, such as yield stress, σ_y, ultimate tensile stress, σ_{UTS}, total elongation, ε_{Total}, and reduction in area, R_A, were almost the same despite the difference of the strain rate. Furthermore, no stress corrosion cracking has been observed with the specimens showing ductile fracture mode. The above suggests that the susceptibility to SCC of F82H is low at these test conditions.

The susceptibility of ODS steels to SCC was evaluated by means of slow strain rate tests (SSRT) in the loop system of hot pressurized water at 288 °C at the pressure of 7.8 MPa. Dissolved oxygen (DO) was controlled to be 8 ppm which is larger than BWR condition. Strain rates were in the range from 10^{-4} to 3×10^{-7} s^{-1}. In ODS steels, the ductility did not depend on the strain rate between 10^{-4} to 3×10^{-7} s^{-1}, indicating that the 19Cr–ODS steel and 19Cr–4.5Al–ODS steel show very low SCC susceptibility. The fracture surface observation by SEM revealed that the entire fracture surface showed ductile mode with many dimples. The reduction in area was also large at all the strain rate conditions. For comparison, similar tests were carried out for the sensitized SUS316L, and the sensitization at 700 °C for 100 h caused a remarkable reduction of the total strain that indicated the occurrence of the SCC.

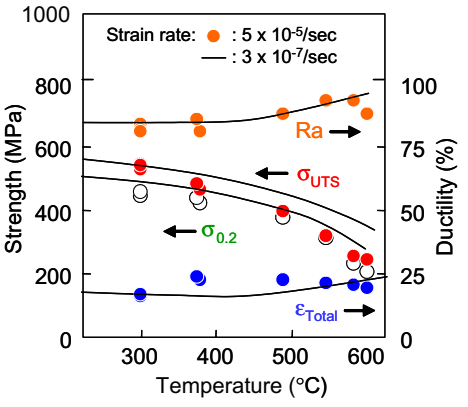

Fig. 8. Tensile properties of F82H deformed at different strain rates.

5.2. Corrosion test

The weight change during the SSRT was measured for F82H at temperatures between 380 and 583 °C, and the results are shown in Fig. 9, indicating that it depends strongly on the test temperature. A similar behavior was observed for JLF-1 that showed a weight gain of 1.7 mg/cm^2 at a pressure of 25 MPa at 510 °C after 200 h elapse [30]. Fig. 10 shows the dependence of weight gains on corrosion test period of the ODS steels [31]. This result indicates that the weight gains of all high-Cr ODS steels are smaller than an austenitic stainless steel (SUS316L). It is noticed that the ODS steel which contained even 14 wt% of Cr showed higher resistance to corrosion than SUS316L that contained 18 wt% Cr and 10 wt% Ni. The ODS steels

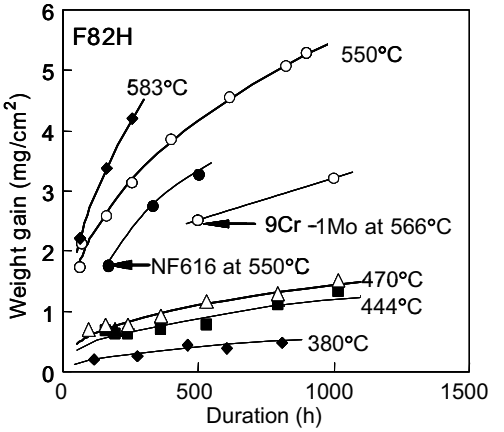

Fig. 9. The weight change during the SSRT of F82H at temperatures between 380 and 583 °C.

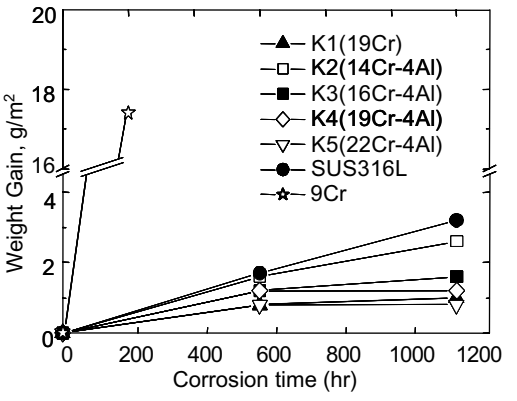

Fig. 10. The dependence of weight gains on corrosion test period of the ODS steels [26].

with higher Cr concentration show better corrosion resistance. However, the weight gain of the 9Cr-steel (JLF1) is much larger than the SUS316L. It is clear that the oxide film of 9Cr martensitic steel consists of multi-layers and is thicker than that of SUS316L, as expected from the weight gain test results. However, the oxide film of the 16Cr–4Al–ODS steel is too thin to distinguish each oxide layer by means of SEM. The oxidation film of SUS316L was very rugged, while those of the ODS steel were very uniform. As for the effect of Al on the corrosion rate, it is too small to cause the difference in the weight gain between the ODS steel with and without Al addition.

6. High-thermal efficiency for DEMO and beyond

6.1. High-temperature strength

An increase in the Cr content (19Cr) increased the tensile stress of 9Cr–ODS steel. This can be explained by solid solution hardening by Cr. The tensile stress was larger than 9Cr–ODS by about 100 MPa at temperatures between RT and 400 °C, and about 50 MPa at 800 °C. Since the potential hardening by oxide dispersion is much larger than that by solid solution of Cr, the difference in the tensile stress due to increasing Cr is somewhat smaller than the difference in the tensile stress between ferritic steel and 9Cr–ODS steel.

A coupling of RAFS and ODS steel could be effective to construct highly efficient and realistic fusion blankets.

6.2. Potential of aging embrittlement

Since the increase in Cr concentration to over 14 wt%Cr often causes aging embrittlement due to formation of Cr-rich secondary phases, the effects of aging on tensile properties were investigated after aging at 500 °C for 1000 h. The test temperature was RT and the deformation rate was 0.5 mm/min. Although the aging caused an increase in the yield stress, almost no effect was observed for the total strain of all the steels. The hardening was larger in higher Cr content ODS steels. The DBTT shifted to high temperature by about 40 °C and 70 °C in the 19Cr–4Al–ODS and 19Cr–ODS steel, respectively. In contrast to this, the 16Cr–4Al–ODS steel never showed the DBTT shift even after the aging at 500 °C for 4800 h.

Table 3
Summary of the effects of aging on the 19Cr–ODS steel

	Age hardening (MPa)	Reduction of elongation	ΔDBTT	TEM
14Cr–4AI	42.1	No change	~0	–
16Cr–4AI	34.6	No change	~0	α′-phase
19Cr–4AI	168	Small	70 K	α′-phase

To make clear the mechanism of the aging embrittlement, the microstructure of 19Cr–ODS steel was observed by transmission electron microscope (TEM) before and after the aging at 500 °C for 1000 h. In the as-received condition, fine oxide particles were observed in the matrix, while many larger structures as well as oxide particles were observed after aging. Since the diffraction patterns of the aged sample did not show any extra spots besides those due to oxide particles, the structures were assumed to be Cr-rich phases which had BCC structure with almost the same lattice parameter as iron. The hardening observed for the aged specimen appears to be interpreted in terms of precipitation hardening by Cr-rich phases.

The effects of aging on the 19Cr–ODS steel are summarized in Table 3, indicating that 14Cr and 16Cr–ODS steels suffer no aging embrittlement after the aging at 500 °C for 1000 h, while 19Cr–ODS showed a remarkable embrittlement. It is interesting that Cr-rich α′ phases were observed in 16Cr–ODS steel that did not suffer any aging embrittlement. It was reported that the formation of Cr-rich α′ can be influenced by the third element of the steels [32]. A more precise correlation study is necessary to understand the role of Cr-rich α′ phases in the aging embrittlement.

7. Concluding remarks

US–Japan collaborative research on ferritic steels R&D has been successfully provided an irradiation database utilizing HFIR. Recent results clearly showed that the mechanism of irradiation embrittlement of two Japanese RAFSs were different from each other. The larger DBTT shift observed in F82H is interpreted in terms of both the matrix hardening mechanism and reduction of cleavage fracture stress along lath block and packet boundaries, while that of JLF-1 is due to only the hardening effect. The reduction of lath block and packet boundary fracture stress is con-

sidered to be due to $M_{23}C_6$ carbide precipitation of which the morphology can be controlled by thermal heat treatment. Dimensional change measurement during in-pile creep tests revealed the creep strain was limited at 300 °C. Materials performance of welds under neutron irradiation will be critical to determine the life time of blanket structural components. Further irradiation experiments and database development is necessary. Corrosion tests have been done for F82H. High Cr–ODS steels showed higher resistance to corrosion than austenitic stainless steel, SUS316L. Application of ODS steels to a fusion blanket is essential to increase the thermal efficiency of the blanket systems beyond DEMO. A coupling of RAFS and ODS steel could be effective to construct a highly efficient and realistic fusion blanket.

Acknowledgements

A part of this work is supported by US–Japan collaborative researches, DOE/JAERI and DOE/MEXT for the irradiation experiment, and by METI for the ODS steel R&D.

References

[1] Minutes of 13th Test Blanket Working Group (TBWG-13), ITER-JWS, Garching, (2004).
[2] Minutes of 12th Test Blanket Working Group (TBWG-12), ITER-JWS, Garching, (2003).
[3] C.P.C. Wong et al, J. Nucl. Mater., these Proceedings, doi:10.1016/j.jnucmat.2007.03.241.
[4] M. Enoeda et al., Nucl. Fus. 43 (12) (2003) 1837, and <http://stacks.iop.org/0029-5515/43/1837>.
[5] L.V. Boccaccini, L. Giancarli, G. Janeschitz, S. Hermsmeyer, Y. Poitevin, A. Cardella, E. Diegele, J. Nucl. Mater. 329–333 (2004) 148.
[6] L. Giancarli, J.P. Bonal, A. Caso, G. Le Marois, N.B. Morley, J.F. Salavy, Fus. Eng. Des. 41 (1998) 165.
[7] ARIES-Team, D.K. Sze, Fus. Eng. Des. 41 (1998) 371.
[8] A. Sagara, O. Motojima, K. Watanabe, S. Imagawa, H. Yamanishi, O. Mitarai, T. Satow, H. Tikaraishi, Fus. Eng. Des. 29 (1995) 51.
[9] M.A. Sokolov, R.L. Klueh, G.R. Odette, K. Shiba, H. Tanigawa, 21st Inter. Symp., ASTM STP 1447 (2004) 408.
[10] A. Kimura, H. Kayano, S. Ohta, J. Nucl. Mater. 179–181 (1991) 741.
[11] H. Kayano, A. Kimura, M. Narui, T. Kikuchi, S. Ohta, J. Nucl. Mater. 179–181 (1991) 671.
[12] R.L. Klueh, D.S. Gelles, S. Jitsukawa, A. Kimura, G.R. Odette, B. van der Schaaf, M. Victoria, J. Nucl. Mater. 307–311 (2002) 455.
[13] B. van der Schaaf, D.S. Gelles, S. Jitsukawa, A. Kimura, R.L. Klueh, A. Moslang, G.R. Odette, J. Nucl. Mater. 283–287 (2000) 52.
[14] R.L. Klueh, P.J. Maziasz, J. Nucl. Mater. 187 (1992) 43.
[15] D.S. Gelles, G.L. Hanki, M.L. Hamilton, J. Nucl. Mater. 258–263 (1998) 1216.
[16] A. Kimura, R. Kasada, R. Sugano, A. Hasegawa, H. Matsui, J. Nucl. Mater. 283–287 (2000) 827.
[17] A. Kimura, R. Kasada, K. Morishita, R. Sugano, A. Hasegawa, K. Abe, T. Yamamoto, H. Matsui, N. Yoshida, B.D. Wirth, T.D. Rubia, J. Nucl. Mater. 303–307 (2002) 521.
[18] A. Kimura, H. Kayano, T. Misawa, H. Matsui, J. Nucl. Mater. 212–215 (1994) 690.
[19] A. Kimura, Fus. Sci. Tech. 44 (2) (2003) 480.
[20] R. Kasada, T. Morimura, H. Matsui, M. Narui, A. Kimura, 19st Inter. Symp., ASTM STP 1366 (2000) 448.
[21] R. Kasada, A. Kimura, Mater. Trans. 46 (3) (2005) 475.
[22] H. Tanigawa et al., Fus. Sci. Technol. 44 (2003) 206.
[23] H. Tanigawa, H. Sakasegawa, R.L. Klueh, Mater. Trans. 46 (3) (2005) 469.
[24] E. Wakai, T. Taguchi, T. Yamamoto, H. Tomita, F. Takada, S. Jitsukawa, Mater. Trans. 46 (3) (2005) 481.
[25] H. Ogiwara, H. Sakasegawa, H. Tanigawa, M. Ando, Y. Katoh, A. Kohyama, J. Nucl. Mater. 307–311 (2002) 299.
[26] H. Ogiwara et al., private communication.
[27] T. Morimura, A. Kimura, H. Matsui, J. Nucl. Mater. 239 (1996) 118.
[28] A. Kimura, T. Suzuki, M. Jincho, H. Matsui, 18st Inter. Symp., ASTM STP 1329 (1998) 110.
[29] T. Suzuki, K. Itoh, Y. Naruse, H. Matsui, A. Kimura, 19th Inter. Symp., ASTM STP 1366 (2000) 266.
[30] T. Hirose et al., J. Nucl. Mater., these Proceedings, doi:10.1016/j.jnucmat.2007.03.212.
[31] H.S. Cho et al., J. Nucl. Mater., these Proceedings, doi:10.1016/j.jnucmat.2007.03.211.
[32] M.H. Mathon, Y. de Carlan, G. Geoffroy, X. Averty, A. Alamo, C.H. de Novin, J. Nucl. Mater. 312 (2003) 236.